Supplementary Information for

A Human Lymph node-on-a-Chip for Personalized Evaluation of Vaccine Immunogenicity

The Supplementary Information file includes:

Supplementary Methods

Figs. S1 to S6

Tables. S1 to S4

I. Supplementary Methods

Mesenteric lymph node tissue samples

Human mesenteric lymph nodes were obtained from patients undergoing gastrointestinal surgery at NYU Langone Health. All procedures involving human tissues were approved by the Institutional Review Board at NYU, and were conducted in accordance with the principles of the Declaration of Helsinki. All participants provided written informed consent. To ensure compliance with the HIPAA regulations, all of the samples were deidentified before analysis. Briefly, human lymph nodes were dissected from mesenteric tissue immediately post-resection and transferred on ice to the laboratory. For histology analysis, human lymph node tissues were sectioned to 5 μm thickness using a cryostat (Leica Biosystems) and immediately fixed in 4% paraformaldehyde (Alfa Aesar) for 15 minutes at room temperature. Fixed sections were washed with phosphate buffered saline (PBS, Thermo Fisher Scientific) and stored at 4 °C until subsequent immunostaining was performed within 24 hours. For scRNA-seq analysis, tissues were minced and or were enzymatically dissociated using Collagenase/Dispase (Sigma) for 30 minutes at 37 °C with gentle agitation. The dissociated cells then were filtered through a 70 μm strainer (Corning), washed with cold PBS, then centrifuged at 300×g for 8 minutes at 4 °C. The resulting cell suspensions were cryopreserved in freezing medium (Gibco) and stored in liquid nitrogen for subsequent scRNA-seq using the 10× Genomics platform.

Immunofluorescence staining of lymph node tissue

Fixed human lymph node tissue sections were permeabilized with 0.1% Triton X-100 (Sigma-Aldrich) in PBS for 15 minutes, and blocked with a blocking solution of 5% bovine serum albumin (BSA, Sigma) in PBS for 1 hour at room temperature. Sections were then incubated with the primary antibodies diluted in blocking solution overnight at 4°C. The following primary antibodies were used to identify different cell components in the lymph node tissues: anti-CD3e for T cell, anti-PAX5 for B cell, anti–α-smooth muscle actin (αSMA) for lymphatic endothelial cell, anti-CD31 for endothelial cell, anti-CD163 for macrophage, anti-HLA-DR to label MHC class II^+ antigen-presenting cells, such as dendritic cells. After primary antibody incubation, sections were washed three times with PBS and then incubated with fluorophore-conjugated secondary antibodies for 1 hour at room temperature in the dark. Nuclei were counterstained with DAPI for

5 minutes, followed by another series of PBS washes. Slides were mounted with an anti-fade mounting medium (ProLong™ Gold Antifade Mountant, Thermo Fisher Scientific). Fluorescence images were acquired using a fluorescence microscope (Axio Observer 7; Carl Zeiss, Germany). Antibody sources and dilution information are provided in **Supplementary Table S4**.

Time-lapse tracking of T cell migration

To visualizing the cell activities on chip, DCs, T cells, and FRCs were pre-labeled with DiO, DiD, and CellTrace Violet cell labeling solutions (Thermo Fischer Scientific), respectively. RFP expressing HUVECs (Angio-Proteomie) were used to form the HEVs on chip. After 5 days culture, phase contrast and fluorescence images of the chips were captured every 5 minutes over a 4-hour period using a 20x objective under an inverted microscope (Zeiss Axio Observer.Z1) equipped with an environmental control incubator (Okolab) at 37°C and 5% CO_2. T cell motility were assessed by manually tracking individual T cells (>100 cells per condition) in ImageJ (NIH) using the Manual Tracking plugin.

Flow cytometry

Human immune cells isolated from PBMCs or single-cell suspensions recovered from the chip with nattokinase (50 Fu/mL, NSK-SD, Pure Encapsulations) were analyzed by flow cytometry. For staining of human cell surface marker proteins, the cells were incubated on ice for 15 minutes in staining buffer (BioLegend) with fluorescently-labeled antibodies (BioLegend, details see **Supplementary Table S4**) based on the manufacturer's recommendations. Cells were washed three times and stained with 7-AAD (Thermo Fisher Scientific) to exclude dead cells, washed twice with flow cytometry washing buffer and resuspended in 200 µL of cell staining buffer for flow cytometric analysis using on FACSCanto™ Flow Cytometry (BD Biosciences). Subsequent analysis was done using FlowJo software version 10 (Treestar, BD Biosciences). The fluorescence calibration was adjusted by incubating respective antibodies with OneComp eBeads compensation beads (Invitrogen). Specifically, imDCs ($CD11c^+CD1a^+$), mDCs ($CD11c^+CD80^+CD83^+HLA\text{-}DR^+$), total B cells ($CD3^-CD19^+$), naïve B cells ($CD19^+CD27^-CD38^-$), pre-GC B cells ($CD19^+CD27^-CD38^+$), GC B cells ($CD19^+CD27^+CD38^+$), memory B cells ($CD19^+CD27^+CD38^-$), plasma cells ($CD19^+CD27^+CD38^{++}$) were identified by selecting living cells that tested positive for these surface markers in flow cytometry analyses.

Quantification of B cell subsets by CD27 and CD38 expression

To track B cell differentiation in response to vaccination, the lymph node chips were fixed at defined time points and stained with CD27 and CD138 to distinguish different B cell subsets. All fixed chips were immunostained simultaneously on the same day under identical antibody concentrations, incubation times, and imaging conditions to ensure consistency across chips. Confocal microscopy was performed using uniform laser power, gain, and exposure settings to enable direct comparison of fluorescence intensities. B cell subsets were distinguished using CD27 and CD138 to identify memory and plasma cells. For further characterization of B cell maturation, CD27 and CD38 staining was used to define naïve B cells ($CD27^{-}CD38^{-}$), pre-GC B cells ($CD27^{-}CD38^{+}$), GC B cells ($CD27^{+}CD38^{+}$), memory B cells ($CD27^{+}CD38^{-}$), and plasma cells ($CD27^{+}CD38^{++}$). B cells were identified as $CD19^{+}$ populations, while $CD19^{-}$ cells in the same field of view were used as internal negative controls for background signal estimation. To allow consistent comparison across time, fluorescence intensities from $CD19^{+}$ B cells and $CD19^{-}$ collected at all time points were pooled to establish unified thresholds for CD27 and CD38 expression. The mean and standard deviation of CD27 and CD38 fluorescence intensities were calculated from pooled $CD19^{+}$ cells across all time points. Cells were categorized as $CD27^{+}$ or $CD38^{+}$ based on thresholds exceeding the pooled CD27 mean or CD38 mean, respectively, and as $CD38^{++}$ if exceeding the mean plus two standard deviations. Scatter plots of CD27 vs. CD38 were generated for each time point to visualize subset distributions. The percentage of cells within each subset gate was quantified using Matlab R2024b.

Antibody detection by multiplex influenza immunoassay

To assess influenza-specific antibody secretion levels in on-chip cultures and matched clinical serum samples, we used a custom-designed, bead-based multiplex antigen binding assay on the Luminex™ platform, which we ran in a 26-plex comprising 23 recombinant HA and NA antigens derived from historical and concurrent influenza A and B virus strains, complemented with Rubella Virus E1/E2 (ACROBiosystems) and BSA (Fisher Scientific) negative control antigens, as well as IC45 uncoupled, autofluorescing positive control beads (Luminex, MagPlex RP1 Monitor beads) (**Supplementary Table 2**). Recombinant HA and NA proteins were obtained from commercial sources (Sino Biological or, for clade 2.3.4.4b H5 and N1 antigens, from BEI Resources) and coupled to magnetic, fluorescently labeled MagPlex microsphere beads (Luminex)

10-100 pmol per 106 beads using the xMAP Antibody Coupling Kit (Luminex), which utilizes carbodiimide coupling to primary amines of the antigens. Culture supernatants were collected from each chip on day 10 post-vaccination, matched serum samples from the same donors were collected before vaccination and approximately one month after influenza vaccination. Samples were stored at −80 °C and were thawed on ice before analyses.

Coupling was confirmed using a positive control serum pool from the NYU Langone Vaccine Center Biorepository and a biotinylated rabbit anti-human IgG (H+L) detection antibody (Abcam) at a concentration of 2 µg/mL. All influenza antigens were His-tagged, and coupled beads were additionally confirmed using a biotinylated anti-His antibody (Abcam) at a 1:2000 dilution. These antibodies were also used to confirm the absence of cross-reactive antibody responses to the antigens in multiplex (all antigens in a single well) versus singleplex (only one antigen per well) measurements. Sera were heat-inactivated at 56°C for 30 minutes, then incubated with multiplexed, antigen-coupled beads in PBS with 0.01% BSA (Sigma-Aldrich) and 0.02% Tween-20 (Sigma-Aldrich) for one hour at room temperature in the dark with shaking at 800 rpm. Serum samples were analyzed at final dilutions of 1:100 and 1:2000. Beads were rinsed twice in PBS-TB using a plate magnet and subsequently incubated for 30 minutes at room temperature with the biotinylated rabbit anti-human IgG (H+L) detection antibody, followed by incubation with 4 µg/mL streptavidin-PE for 30 minutes under the same conditions. After final rinsing, beads were resuspended in PBS-TB and analyzed using a Luminex 200 instrument with standard settings. To correct each sample for unspecific binding to beads, we normalized the data using the IC45 bead reading. The final binding area under the curve (AUC) was calculated by summing median fluorescence intensities (MFIs) from both dilutions. Batch normalization was done for each antigen using the average signals obtained with the positive control pool. These corrections reduced technical variability while preserving biological trends.

To specifically evaluate responses to vaccine-matched strains, we focused on the four HA antigens corresponding to the 2022–2023 seasonal influenza vaccine formulation: A/Wisconsin (H1N1), A/Darwin (H3N2), B/Austria (B/Victoria lineage), and B/Phuket (B/Yamagata lineage). Fold change in IgG response was computed for each donor by dividing the post-vaccination signal by the corresponding pre-vaccination baseline.

Scanning electron microscopy

To facilitate downstream sectioning for SEM imaging, the bottom glass substrate of the lymph node chip was replaced with a 2 mm-thick PDMS layer during device fabrication. On day 10 post-vaccination, chips were washed three times with PBS (10 minutes each wash) and fixed in 10% neutral buffered formalin (4% formaldehyde, 1% methanol in phosphate buffer; Electron Microscopy Sciences) at 4 °C for 3 hours. Fixed chips were washed again three times with PBS (10 minutes each wash) and sectioned into 2 mm-thick slices. Samples were dehydrated through a graded ethanol series (30%, 50%, 70%, 80%, and 90%; Cat#E7023, Sigma-Aldrich) for 10 minutes each, followed by three incubations in 100% ethanol for 20 minutes each. Dehydrated sections were subjected to critical point drying using a critical point dryer (Tousimis Samdri-931). Samples were mounted onto SEM stub with carbon tape (Electron Microscopy Sciences) and sputter-coated with gold for 30 seconds (~15 nm thickness) in a sputter coater (108 Auto, Cressington Scientific Instruments). Imaging was performed using a variable pressure SEM (S-3400N, Hitachi High-Technologies) under high vacuum at 15 kV.

scRNA-seq analysis

For scRNA-seq analysis, single-cell suspensions were generated from freshly thawed PBMCs, human lymph node tissue, or recovered from the lymph node chips treated with human seasonal influenza vaccines for 10 days or left untreated (designated as Vaccine and None) using nattokinase (50 Fu/mL, NSK-SD, Pure Encapsulations). Different batches of single-cell suspensions were pre-labeled with different anti-human hashtag antibodies (TotalSeq, BioLegend), i.e., Hashtag5- AAGTATCGTTTCGCA, Hashtag6-GGTTGCCAGATGTCA, Hashtag7-TTCCGCCTCTCTTTG, Hashtag8-AGTAAGTTCAGCGTA, all at 1:250 dilution and mixed into one sample. Cells were barcoded using TotalSeq-A hashtag antibodies, pooled, and processed with the Chromium Single Cell 3′ v3 platform (10x Genomics). Libraries were sequenced on an Illumina NovaSeq 6000.

The raw reads from the 10x Genomics platform were processed in the CellRanger pipeline (version 6.1.2) with hg38/GRCh38 as the reference genome for read alignment. Further analyses including quality control and data filtering, the identification of highly variable genes, dimensionality reduction, standard unsupervised clustering algorithms, and the discovery of differentially expressed genes were performed using the R package Seurat (version 4.2.1/5.0).

Hashtag demultiplexing was performed using Seurat's HTODemux (positive.quantile = 0.99), assigning each cell to Hashtag 5, Hashtag 6, Hashtag 7, or Hashtag 8 and removing multiplets and negatives. Gene expression data were analyzed using Seurat (v5.0, R v4.2.1). Samples were integrated using PCA-based anchors (dims = 1:30), or alternatively mapped to Hashtag 7 (vaccinated chip) via label transfer (MapQuery). Differentially expressed genes between clusters or hashtags were identified using Wilcoxon tests (Bonferroni-adjusted $p < 0.05$, $\log_2FC > 0.25$), and functional annotation was performed with clusterProfiler (v4.4.4). Cell types were annotated using canonical markers and reference datasets. Lineage-specific trajectories were reconstructed with Monocle 3 (v1.2.9). All analyses were performed in R (v4.2.1).

For inter-donor comparisons, cells from defined immune lineages were aggregated into donor-level pseudobulk profiles and analyzed using edgeR to identify differentially expressed genes, which were visualized as z-score–scaled heatmaps with hierarchical clustering. Pathway activity was assessed by gene set enrichment analysis (GSEA) using MSigDB Hallmark pathways, including MYD88 and IL2–STAT5 signaling, in a cell-type–resolved manner and summarized as dot plots. In addition, enrichment of APRIL–TACI signaling was evaluated using a custom gene set (TACI_SIGNALING_CORE; TNFRSF13B, TNFSF13, TNFSF13B, TRAF2, TRAF3, TRAF6, BIRC3, MAP3K14, NFKB1, NFKB2, RELA, RELB, NFKBIA, PIK3CD, PIK3R1, AKT1, and MTOR) and visualized using donor-level GSEA enrichment curves.

II. Supplementary Figures

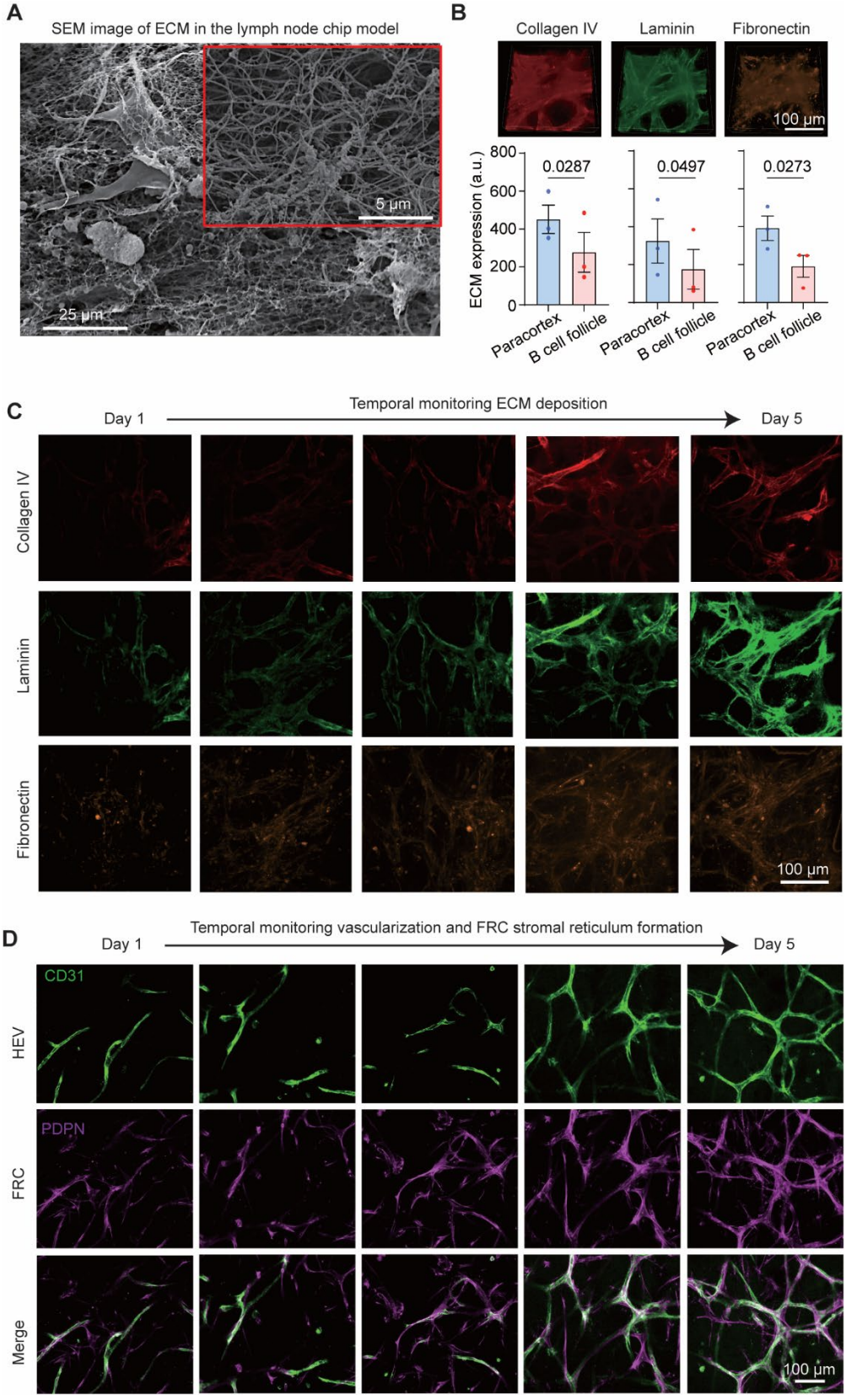

Fig. S1. ECM and stromal reticulum formation in the LN-on-a-chip. (**A**) Representative SEM images showing ECM in the lymph node chip model showing a dense, fibrillar matrix that supports 3D cellular organization. The magnified inset highlights the nanoscale fibrous ECM network. (**B**) Representative immunofluorescence images and quantification of ECM proteins (collagen IV, laminin, fibronectin) in the paracortical and B cell follicular regions of the lymph node chip on day 10. ECM deposition was significantly higher in the paracortex than the B cell follicle, suggesting stromal network heterogeneity. (**C**) Time-lapse confocal imaging showing progressive accumulation of Collagen IV, Laminin, and Fibronectin within the stromal reticulum from day 1 to day 5 (identical imaging settings across time points). (**D**) Time-lapse confocal imaging showing the progressive formation of $CD31^+$ vascular and $PDPN^+$ FRC networks and alignment within the paracortical region.

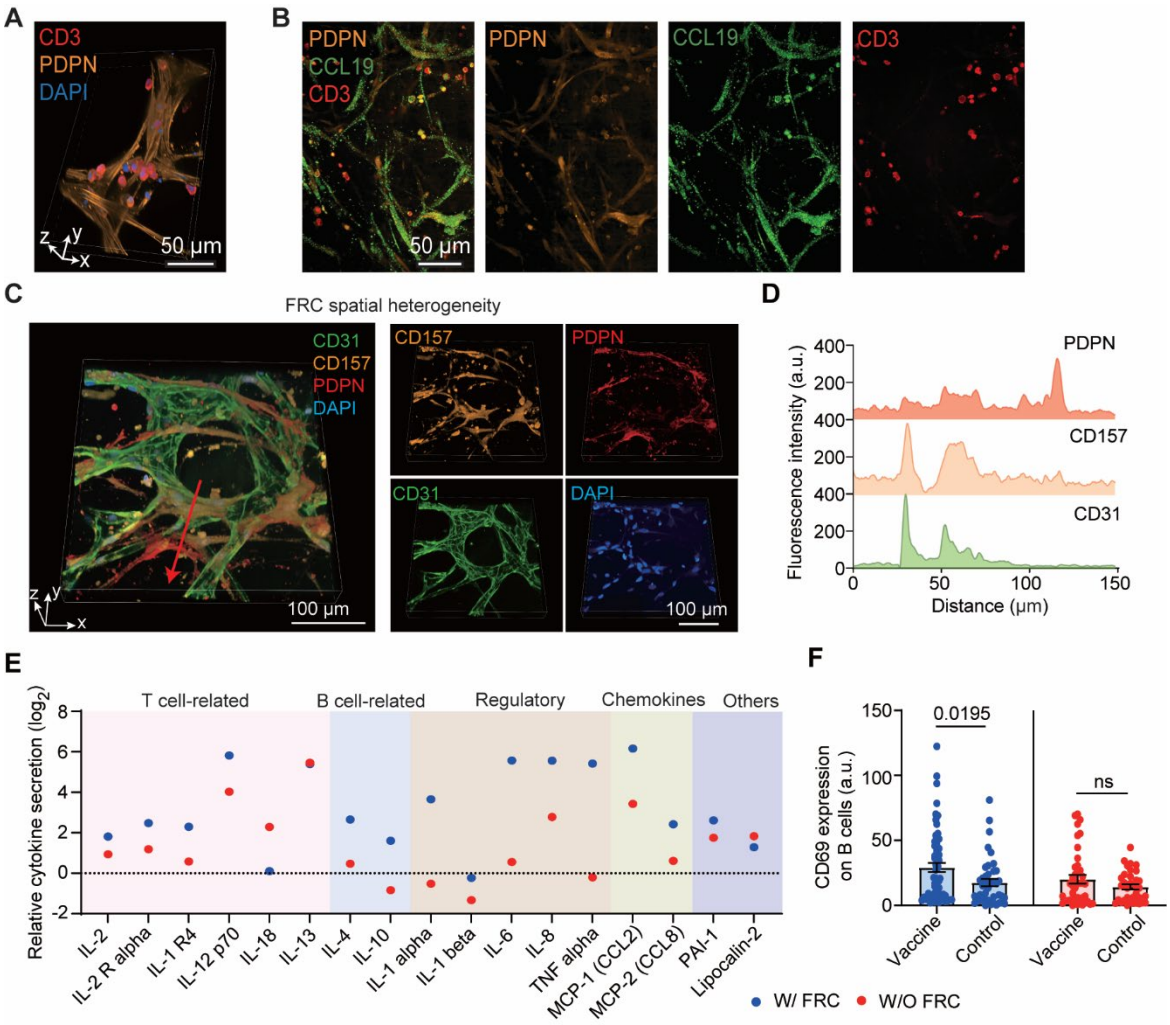

Fig. S2. FRC network supports T cell localization and activation on chip. (**A**) Representative immunofluorescence 3D reconstruction images showing CD3⁺ T cells in close proximity to the PDPN⁺ FRC network within the paracortex. Nuclei, DAPI. (**B**) Immunofluorescence images showing CCL19 localized along the PDPN⁺ FRC scaffold adjacent to CD3⁺ T cells, demonstrating chemokine-mediated guidance of T cell positioning. For A-B, images were taken on day 10. (**C**) Immunofluorescence 3D reconstruction images of stromal architecture on day 5 reveals spatial heterogeneity of FRC subsets. Classical PDPN⁺ FRCs and CD157⁺ vascular-associated FRCs are organized in distinct niches relative to CD31⁺ vasculature. (**D**) Fluorescence intensity profile along the red arrow in (C) path quantifies the spatial distribution of PDPN, CD157, and CD31. For C-D, images were taken on day 5. (**E**) Cytokine secretion profiles in chips with (blue) or without (red) FRCs on day 10, measured using the Human Immune Response Array C1. Log_2-fold changes show enhanced secretion of T cell–related, B cell–related, regulatory, and chemokine cytokines in the presence of FRCs. (**F**) Comparison of B cell activation levels (CD69) after vaccination with control group on day 10, with or without FRCs (3 independent chips per condition).

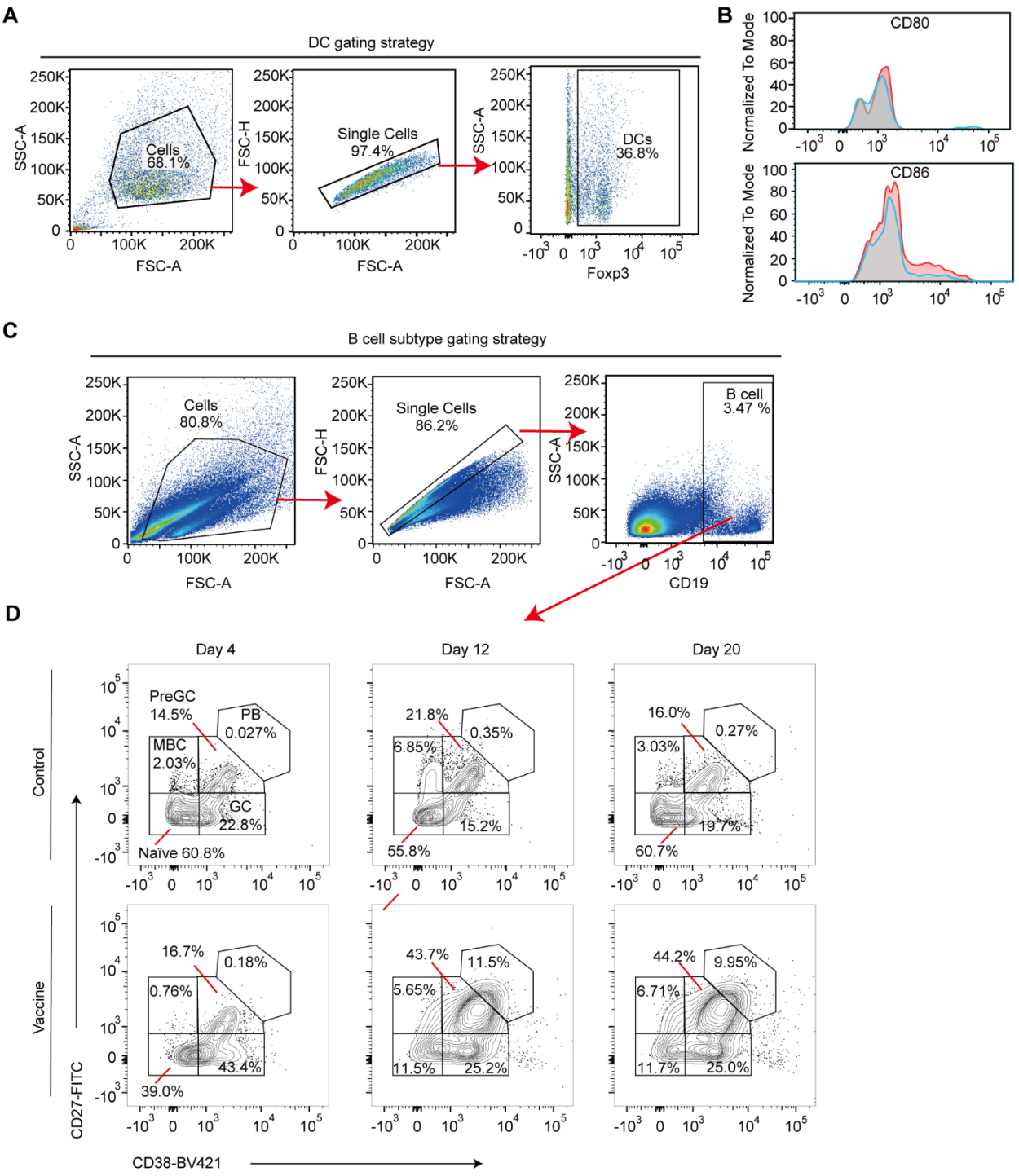

Fig. S3. Characterization of DCs and B cell subsets recovered from LN-on-a-chip cultures by flow cytometry. (**A**) Representative flow cytometry gating strategy for isolating live single cells recovered from LN-on-a-chip cultures. Forward scatter (FSC-A/H) and side scatter (SSC-A) parameters were used to select viable single-cell populations for downstream analysis. (**B**) Histogram plots showing expression of DC activation markers CD80 and CD86 on chip-derived DCs. Data are normalized to mode fluorescence intensity. (**C**) Gating strategy for B cell subset identification using cells collected from LN-on-a-chip cultures. (**D**) Representative flow cytometry

plots showing B cell subset distribution in control and vaccine-stimulated LN-on-a-chip conditions on day 12. $CD19^+$ B cells were further subdivided based on CD27 and CD38 expression into naïve ($CD27^-CD38^-$), pre-GC ($CD27^-CD38^+$), GC ($CD27^+CD38^+$), memory (MBC, $CD27^+CD38^-$), and plasmablast (PB, $CD27^+CD38^{++}$) populations. Percentages indicate the relative frequency of each B cell subset among total $CD19^+$ cells.

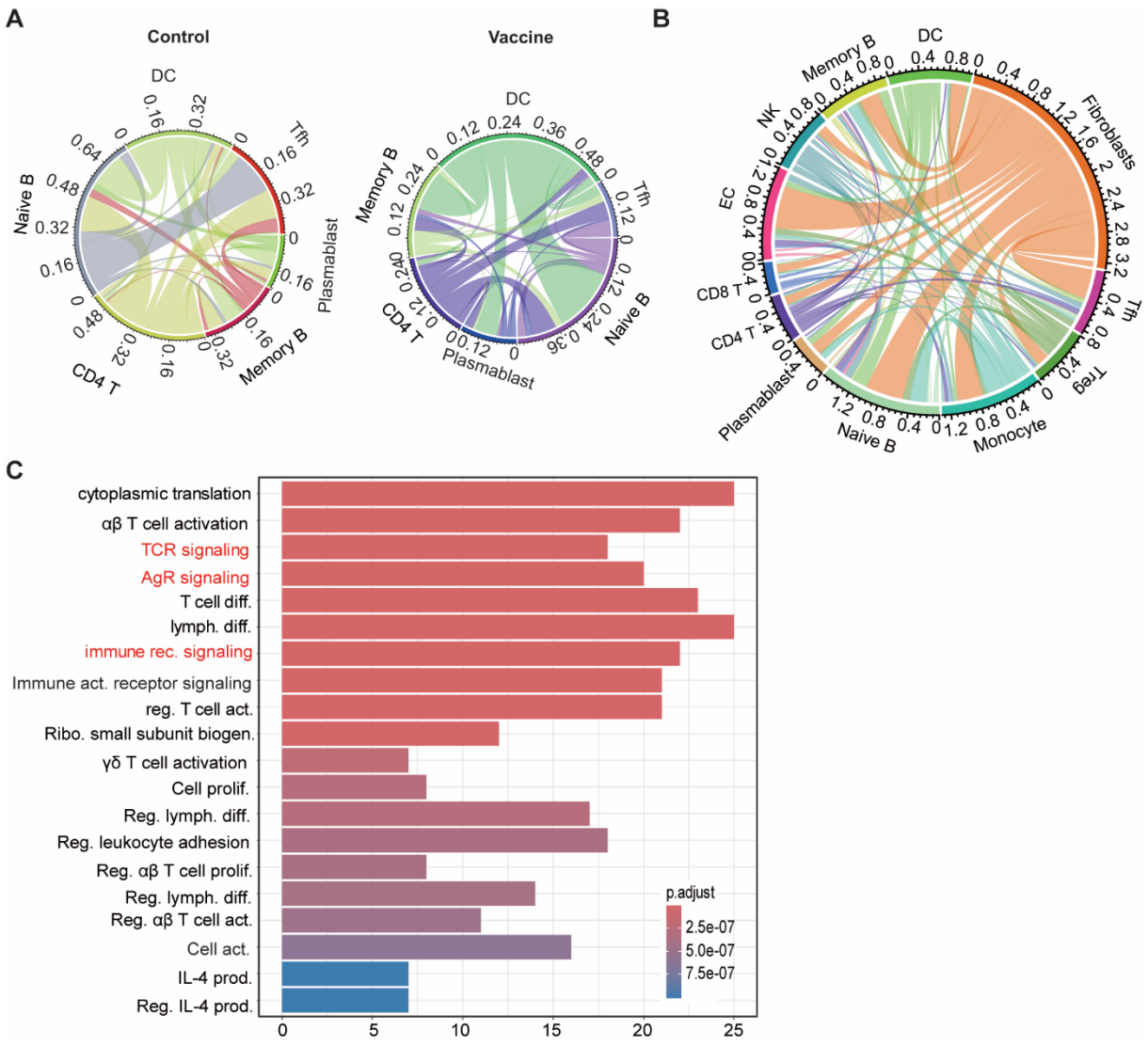

Fig. S4. Vaccine-induced remodeling of intercellular communication networks and functional gene enrichment. scRNA-seq was performed on cells harvested from LN-on-a-chip cultures on day 10 with and without vaccination. (**A**) Chord diagrams of the four selected ligand–receptor pairs (CCL3–CCR1, SPP1–CD44, CD6–ALCAM, FN1–ITGA4/ITGB1) across all final_cell_type groups, for Control (left) and Vaccine (right). Arc segments represent cell types defined by final_type; chord thickness scales with interaction strength (p.adjust<0.05, mean>0.35). (**B**) Representative global cell–cell communication diagram summarizing significant interactions among all annotated cell types (see Methods for aggregation). Outer scales indicate cumulative interaction strength per cell type; chord width reflects relative interaction probability. (**C**) Gene Ontology (Biological Process) enrichment of vaccine-induced genes. Bars show the top terms ranked by gene count; color encodes adjusted p values.

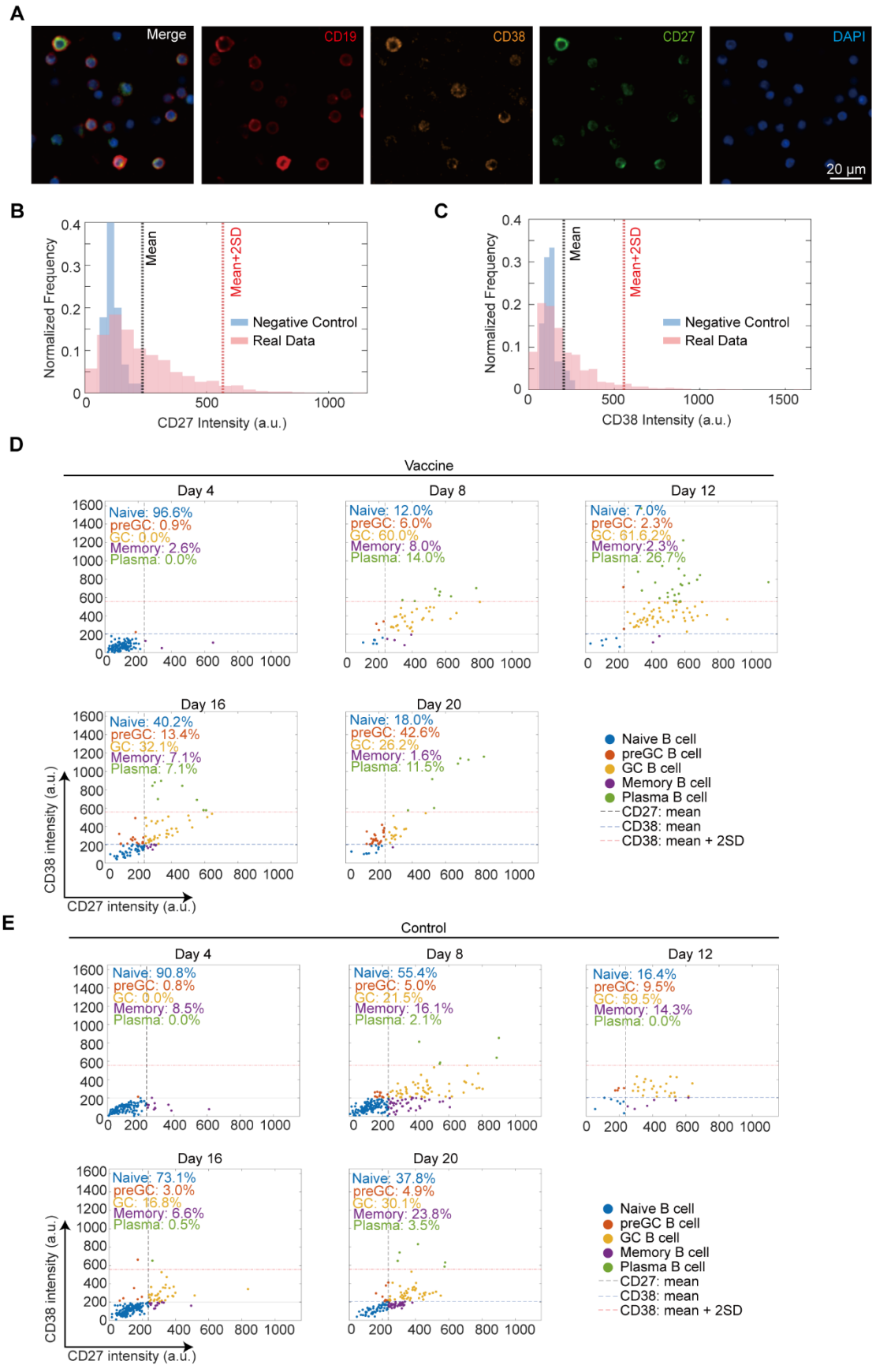
A
Merge
CD19
CD38
CD27
DAPI
20 μm
B
Normalized Frequency
Mean
Mean+2SD
Negative Control
Real Data
CD27 Intensity (a.u.)
C
Normalized Frequency
Mean
Mean+2SD
Negative Control
Real Data
CD38 Intensity (a.u.)
D
Vaccine
Day 4
Naive: 96.6%
preGC: 0.9%
GC: 0.0%
Memory: 2.6%
Plasma: 0.0%
Day 8
Naive: 12.0%
preGC: 6.0%
GC: 60.0%
Memory: 8.0%
Plasma: 14.0%
Day 12
Naive: 7.0%
preGC: 2.3%
GC: 61.6%
Memory: 2.3%
Plasma: 26.7%
Day 16
Naive: 40.2%
preGC: 13.4%
GC: 32.1%
Memory: 7.1%
Plasma: 7.1%
Day 20
Naive: 18.0%
preGC: 42.6%
GC: 26.2%
Memory: 1.6%
Plasma: 11.5%
CD38 intensity (a.u.)
CD27 intensity (a.u.)
Naive B cell
preGC B cell
GC B cell
Memory B cell
Plasma B cell
CD27: mean
CD38: mean
CD38: mean + 2SD
E
Control
Day 4
Naive: 90.8%
preGC: 0.8%
GC: 0.0%
Memory: 8.5%
Plasma: 0.0%
Day 8
Naive: 55.4%
preGC: 5.0%
GC: 21.5%
Memory: 16.1%
Plasma: 2.1%
Day 12
Naive: 16.4%
preGC: 9.5%
GC: 59.5%
Memory: 14.3%
Plasma: 0.0%
Day 16
Naive: 73.1%
preGC: 3.0%
GC: 16.8%
Memory: 6.6%
Plasma: 0.5%
Day 20
Naive: 37.8%
preGC: 4.9%
GC: 30.1%
Memory: 23.8%
Plasma: 3.5%
CD38 intensity (a.u.)
CD27 intensity (a.u.)
Naive B cell
preGC B cell
GC B cell
Memory B cell
Plasma B cell
CD27: mean
CD38: mean
CD38: mean + 2SD

Fig. S5. Quantitative classification of differentiated B cell subsets on chip based on CD27 and CD38 expression. (**A**) Immunofluorescence images showing B cell subtype identification on chip by CD19, CD38, CD27, and DAPI 12 days after vaccination. (**B-C**) Quantitative classification of B cell subsets based on the CD27 and CD38 expression intensities on individual $CD19^+$ B cells. Histograms show distribution of CD27 and CD38 expression in pooled B cells from all 7 time points (days 0-12) compared to pooled negative controls ($CD19^-$ cells in the same fields of view). Data from all time points were combined to establish consistent thresholds. Dashed lines indicate the mean and mean + two standard deviations (2SD) of the pooled experimental data, which were used as gating thresholds to define B cell subpopulations at each time point. (**D**) Scatter plots of CD27 versus CD38 expressions on B cells at days 0 to 12 upon vaccination. Based on the gating thresholds established in A–C, B cells were classified into five subtypes: naïve B cells ($CD27^-CD38^-$), preGC B cells ($CD27^-CD38^+$), GC B cells ($CD27^+CD38^+$), memory B cells ($CD27^+CD38^-$), and plasma cells ($CD27^+CD38^{++}$). (**E**) Control chips analyzed using the same gating thresholds over the same time course.

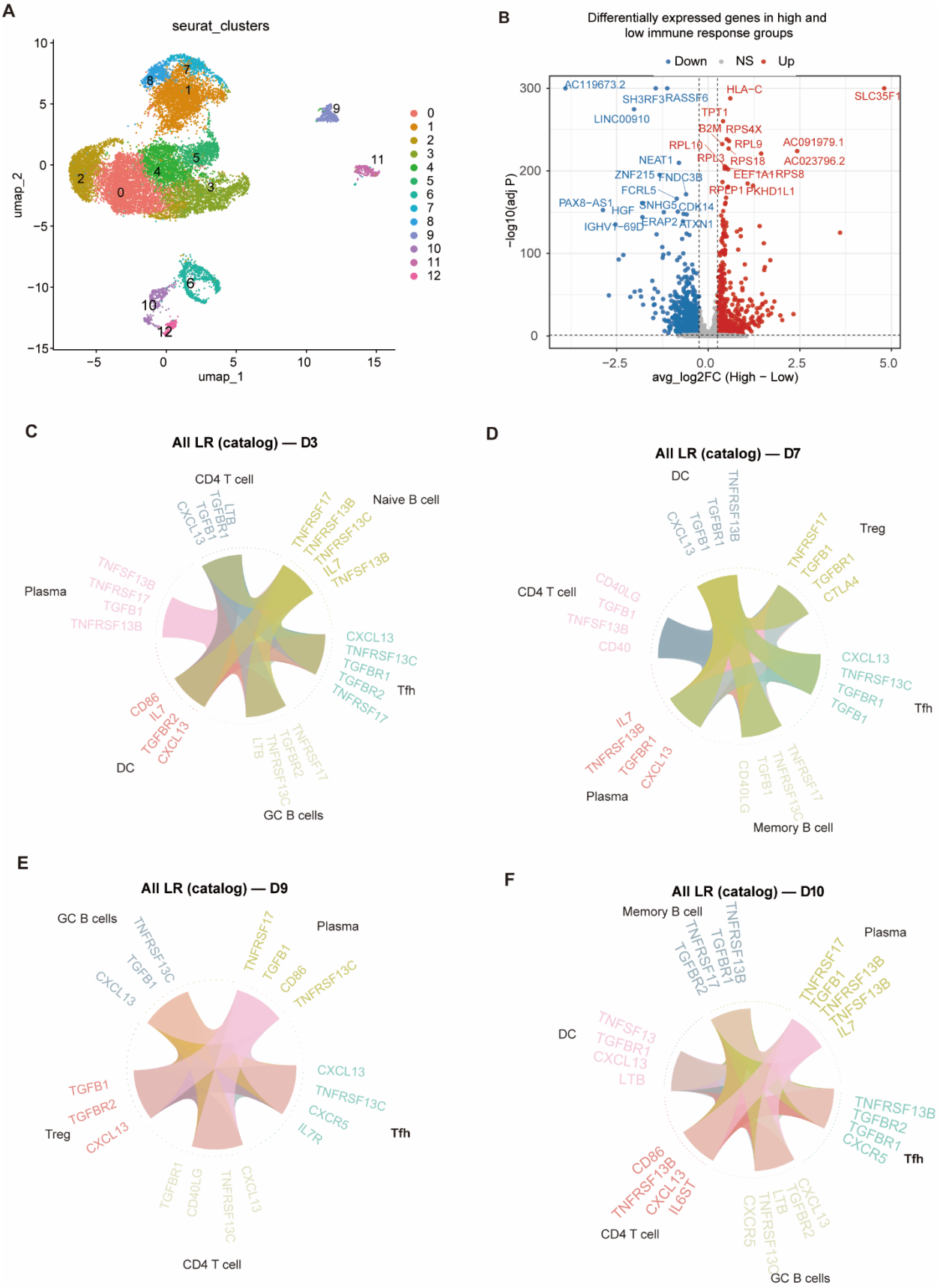
A
seurat_clusters
umap_2
umap_1
0
1
2
3
4
5
6
7
8
9
10
11
12
B
Differentially expressed genes in high and low immune response groups
Down
NS
Up
−log10(adj P)
avg_log2FC (High − Low)
AC119673.2
SH3RF3
RASSF6
LINC00910
HLA−C
SLC35F1
TPT1
B2M
RPS4X
RPL10
RPL9
AC091979.1
NEAT1
RPL3
RPS18
AC023796.2
ZNF215
FNDC3B
EEF1A1
RPS8
FCRL5
RPLP1
FKHD1L1
PAX8−AS1
HGF
SNHG5
CDK14
IGHV1−69D
ERAP2
ATXN1
C
All LR (catalog) — D3
CD4 T cell
Naive B cell
Plasma
Tfh
DC
GC B cells
D
All LR (catalog) — D7
DC
Treg
CD4 T cell
Tfh
Plasma
Memory B cell
E
All LR (catalog) — D9
GC B cells
Plasma
Treg
Tfh
CD4 T cell
F
All LR (catalog) — D10
Memory B cell
Plasma
DC
Tfh
CD4 T cell
GC B cells

Fig. S6. Transcriptional and ligand–receptor features that distinguish high versus low vaccine responders. scRNA-seq analysis (10x Genomics) was performed on chip cultures collected on day 10 post-vaccination from representative high- (D3), intermediate- (D7) and low-response (D9, D10) donors. (**A**) UMAP of all single cells colored by Seurat clusters (0–12). (**B**) Volcano plot comparing high/intermediate responders (D3, D7) versus low responders (D9, D10) across all cells after removing sex-associated genes. X-axis: average log2 fold-change (High–Low); Y-axis: −log10 adjusted P (FDR, Methods). Dots in red and blue, and grey colors denote genes up-regulated, down-regulated and no significant difference in high responders comparing to low responders, respectively. Selected labels highlight markers of antigen presentation (HLA-C, B2M) and translational machinery enriched in high responders, and inhibitory/lncRNA or processing genes (FCRL5, NEAT1, SNHG5, ERAP2) enriched in low responders. (**C–F**) Circular chord diagrams summarizing the cell-surface ligand–receptor (LR) catalogue measured by TotalSeq-A for each hashtag (D3, D7, D9, D10). Chords connect cognate LR pairs detected (interaction score defined in Methods); outer labels list representative ligands/receptors (colors are for visual grouping only). High/intermediate-responder samples (D3, D7) show greater representation of help/activation axes (e.g., ICOS–ICOSL, CD40–CD40LG, CXCL13–CXCR5, and IL-6–IL-6R), consistent with enhanced DC–T_{fh}–B cell cooperation. Low-responder samples (D9, D10) display relatively increased regulatory/checkpoint or TGFB-family interactions (e.g., CTLA4–CD86, TGFB–TGFBR), in line with attenuated effector programs. Only ligand–receptor interactions that passed the statistical significance threshold (FDR < 0.1) are shown in the chord diagrams.

III. Supplementary Tables

Participant	Gender	Age range	Race	Comorbidity	Age score	CSG	CIRS	Risk Group
D1	Male	30-39	Black/African-American	None				Low CIRS
D2	Female	70-79	White/Caucasian	Depression	+		+	Low CIRS
D3	Female	30-39	Black/African-American	Bipolar disorder			+	Low CIRS
D4	Female	30-39	White/Caucasian	Anxiety				Low CIRS
D5	Male	60-69	White/Caucasian	**HTN**, **hypercholesterolemia,** Brain tumor (resolved)	+	+	++	Mid CIRS
D6	Male	70-79	Black/African-American	**BPH**, **COPD**, **HTN**, prostate cancer (resolved), Hep C (resolved), reflux	+	+	++	Mid CIRS
D7	Male	30-39	White/Caucasian	**HIV infection**		+++	+++	High CIRS
D8	Male	70-79	White/Caucasian	**CAD**	+	+	++	Mid CIRS
D9	Male	60-69	White/Caucasian	**Obesity**, **osteoarthritis**, **ASHD**, **HTN,** bariatric surgery, migraines	+	++	+++	High CIRS
D10	Female	20-29	White/Caucasian	**Asthma**		++	++	Mid CIRS
D11	Male	80-89	White/Caucasian	**CKD**, **CAD**, **HTN**, **hyperlipidemia**, **arthritis**, neuropathy, allergies	+	++	+++	High CIRS
D12	Female	40-49	Asian	Ovarian				Low CIRS
D13	Male	30-39	Asian	None				Low CIRS

Supplementary Table S1. Demographic and clinical characteristics of study participants, and CIRS stratification by age and comorbidity. Age score (0–1): age <65 scored 0, age >65 scored 1. Comorbidity Severity Grade (CSG, 0–3) was determined based on the type and severity of chronic conditions recorded for each participant. Low risk: CSG = 0, no chronic disease or only mild, non-immunologic conditions such as anxiety, depression, bipolar disorder, or mild asthma without corticosteroid use. Moderate: CSG = 1, one cardiometabolic or organ-specific chronic condition, or a combination that is clinically stable without overt immunosuppression. High/Immunocompromised (CSG≥2): CSG = 2, multiple cardiometabolic or inflammatory comorbidities, or respiratory/renal disease requiring ongoing clinical management but without a defined severe immunodeficiency. CSG = 3, the presence of HIV infection, a well-established cause of systemic immune impairment. For each donor, the Composite Immuno-Risk Score (CIRS) was calculated as the sum of the age score and the CSG value. Donors were then stratified into three risk categories: Low risk: CIRS ≤ 1, Mid risk: CIRS = 2, High risk: CIRS = 3.

Supplementary Table S2 The formulation of 2022–2023 seasonal influenza vaccine used for each trial participant.

Participant	Vaccine Manufacturer
Donor 1	Fluad Quadrivalent Seqirus, Inc.
Donor 2	Fluzone Quadrivalent Sanofi Pasteur, Inc.
Donor 3	Flucelvax Quadrivalent Seqirus, Inc.
Donor 4	Fluzone Quadrivalent Sanofi Pasteur, Inc.
Donor 5	Fluzone Quadrivalent Sanofi Pasteur, Inc.
Donor 6	Fluzone High Dose Quadrivalent Sanofi Pasteur, Inc
Donor 7	Fluzone Quadrivalent Sanofi Pasteur, Inc.
Donor 8	Fluad Quad Seqirus, Inc
Donor 9	Fluzone High Dose Quadrivalent Sanofi Pasteur, Inc
Donor 10	FluLaval Quadrivalent ID Biomedical Corporation of Quebec
Donor 11	Fluzone High Dose Quadrivalent Sanofi Pasteur, Inc
Donor 12	FluLaval Quadrivalent ID Biomedical Corporation of Quebec
Donor 13	FluLaval Quadrivalent ID Biomedical Corporation of Quebec

Supplementary Table S3 Antigen panel used in the influenza/rubella bead-based multiplex influenza immunoassay, consisting of 23 influenza A/B HA and NA antigens and the Rubella virus E1/E2 control antigen.

HA or NA	Source
A/Wisconsin/588/2019; A/Victoria/2570/2020 (H1) HA	Annual Vaccine
A/Cambodia/e0826360/2020 (H3) HA	Annual Vaccine
B/Washington/02/2019 (Victoria lineage) HA	Annual Vaccine
B/Phuket/3073/2013 (Yamagata lineage) HA	Annual Vaccine
A/Darwin/9/2021 (H3) HA	Annual Vaccine
B/Austria/1359417/2021 (Victoria lineage) HA	Annual Vaccine
A/Victoria/4897/2022 (H1) HA	Annual Vaccine
A/Brevig Mission/1/1918 (H1) HA	1918 Pandemic
A/Japan/305/1957 (H2) HA	1957 Pandemic
A/Hong Kong/1/1968 (H3) HA	1968 Pandemic
A/California/04/2009 (H1) HA	2009 Pandemic
A/Michigan/45/2015 (H1) HA	mRNA HA vaccine
A/Vietnam/1194/2004 (H5) HA	mRNA HA vaccine
A/Shanghai/1/2013 (H7) HA	mRNA HA vaccine
A/Florida HA	Avian influenza (bird flu) outbreak isolate
A/Wisconsin/588/2019; A/Victoria/2570/2020 (N1) NA	Annual Vaccine
A/Cambodia/e0826360/2020 (N2) NA	Annual Vaccine
B/Washington/02/2019 (Victoria lineage) NA	Annual Vaccine
B/Phuket/3073/2013 (Yamagata lineage) NA	Annual Vaccine
A/Darwin/9/2021 (N2) NA	Annual Vaccine
B/Austria/1359417/2021 (Victoria lineage) NA	Annual Vaccine
A/Victoria/4897/2022 (N1) NA	Annual Vaccine
A/Florida NA	Avian influenza (bird flu) outbreak isolate
Rubella virus E1/E2 antigen	control

Supplementary Table S4 Antibodies used for immunofluorescence staining of lymph node-on-a-chip and the human lymph node tissue, and used for flow cytometry profiling.

Immunofluorescence staining of lymph node-on-a-chip					
Antibody	Fluorescence	Dilution	Host	Cat#	Manufacturer
DAPI	Blue	1 μg/mL	-	D1306	Thermo Fisher Scientific
CD31	FITC	1:50	Mouse	303104	Biolegend
CD157	APC	1:50	Rat	382110	Biolegend
Podoplanin (PDPN)	PE	1:20	Rat	NBP203952JF549	Novus Biologicals
CCL19	-	1:100	Rabit	13397-1-AP	Thermo Fisher Scientific
CD11c	FITC	1:50	Mouse	337214	Biolegend
CD86	PE	1:50	Mouse	374205	Biolegend
CD3	APC	1:50	Mouse	317318	Biolegend
CD4	PE	1:50	Mouse	317410	Biolegend
CD8	FITC	1:50	Mouse	344704	Biolegend
CD3	PE	1:50	Mouse	317308	Biolegend
CD25	APC	1:50	Mouse	302610	Biolegend
CD69	PE	1:50	Mouse	310906	Biolegend
CD19	FITC	1:50	Mouse	302206	Biolegend
CD138	PE	1:50	Mouse	352305	Biolegend
CD19	FITC	1:50	Mouse	302206	Biolegend
CD27	FITC	1:50	Mouse	356404	Biolegend
CD38	Brilliant Viole 421	1:50	Mouse	356618	Biolegend
CD19	APC	1:50	Mouse	302212	Biolegend
BCL6	APC	1:50	Rat	358505	Biolegend
IgD	Alexa Fluor 647	1:50	Mouse	324503	Biolegend
Ki-67	FITC	1:50	Mouse	350508	Biolegend
FOXP3	Brilliant Viole 421	1:50	Mouse	320123	Biolegend
CXCR5	Brilliant Viole 421	1:50	Mouse	145511	Biolegend
Laminin	DyLight488	1:100	Mouse	PA5-22901	Thermo Fisher Scientific
Fibronectin	PE	1:50	Mouse	IC1918P	R&D Systems
Collagen IV	Alexa Fluo 647	1:50	Mouse	51-9871-80	Biolegend
Goat anti-rabbit secondary antibody	Alexa Fluor 488	1:500	Goat	A11008	invitrogen
Immunofluorescence staining of lymph node tissue					
CD3e	Alexa Fluor 488	1:100	Mouse	300415	Biolegend
PAX5	Alexa Fluor 594	1:100	Rabbit	NBP2-22157AF594	Novus Biologicals
aSMA	Alexa Fluor 405	1:100	Mouse	53-9760-82	Thermo Fisher
CD31	Alexa Fluor 555	1:50	Mouse	303116	Biolegend
CD163	Alexa Fluor 647	1:50	Mouse	333622	Biolegend
HLA-DR	Alexa Fluor 488	1:50	Mouse	307640	Biolegend

Flow cytometry					
7-AAD	DNA dye	1:20	-	CAT#00-6993-50	Thermo Fisher Scientific
CD3	APC	1:50	Mouse	317318	Biolegend
CD4	PE	1:50	Mouse	317410	Biolegend
CD8	FITC	1:50	Mouse	344704	Biolegend
CD25	PE/Cyanine7	1:50	Mouse	302611	Biolegend
CXCR5	Brilliant Viole 421	1:50	Mouse	145511	Biolegend
FOXP3	Alexa Fluor 647	1:50	Mouse	320213	Biolegend
CD19	BV510	1:50	Mouse	302241	Biolegend
HLA-DR	FITC	1:50	Mouse	327005	Biolegend
CD80	PE/Cyanine7	1:50	Mouse	305217	Biolegend
CCR7	Alexa Fluor 647	1:50	Mouse	353217	Biolegend
CD209	Brilliant Viole 421	1:50	Mouse	330117	Biolegend
CD1a	PE	1:50	Mouse	300106	Biolegend
CD11c	APC/Cyanine	1:50	Mouse	337217	Biolegend